



## HEAT TRANSFER PERFORMANCE THROUGH OBSTACLES TUBE BASED ON SC- CO<sub>2</sub>

Ameer Abed Jaddoa\*, Hussain Saad Abd

*Electromechanical Engineering Department, University of Technology, Baghdad 00964, Iraq*

### ABSTRACT

In this work, the demeanour of heat transfer in a cooled upstanding turbulent flow condition of supercritical carbon dioxide SC- CO<sub>2</sub> was investigated and analyzed. Several scenarios were adopted to handle the experimental data acquired by applying a perpendicular pipe with bending tape used in the examination model. The outcomes were presented using a typical method 'the dimensionless constitution'. Also, a modification was achieved to improve the relationship among the parameters for the processes of up and down flows. The achieved results will help address this research gap on turbulent perpendicular compound heat load based on cooling conditions. Finally, the experimental results demonstrate the influence of buoyancy forces on the heat transfer process.

**Keywords:** Heat transfer, Inflow resistance, Tube with obstacles, SC-CO<sub>2</sub>

### 1. INTRODUCTION

In the last seven decades, a plethora of investigations on supercritical fluids were conducted both theoretically and empirically. Several applications used supercritical fluids in industrial for instance but not limited to material derivation operation, pumps, cooling machines, and electric power station based nuclear. In this respect, a considerable amount of investigations were introduced in terms of shape configuration, inflows methods, horizontal filled-non-filled tubes, and tiny size-porous designs (Jaddoa, 2021a,b,2022). Taking into account the work introduced by (Zahlan, et al., 2015) concerning the CO<sub>2</sub>-cooled directly heated tubes, this empirical work is a continuance of the experimental program implemented at the University of Ottawa. The primary objective of that empirical work is to provide extra data to the table of a trans-critical multi-fluid (Zahlan, et al., 2015) for HT characteristics. Recall that such studies as [Ahmad, et al., 2017] considered the convective HT in SC-CO<sub>2</sub> flows in tubes with and without inflow walls.

Such a kind of fluids were paid attention to recently due to their characteristics such as zero ozone depletion potential and alleviation of exacerbating climate change, and their HT ability (Lorentzen, 1995). The faded fluid and vapour conditions and the influential fluctuations in thermodynamics besides the material properties at diverse heat and pressure degrees are the functions that could be observed at the vital juncture. Figure 1. shows the influence of heat degree on the specific heat  $C_p$ , thermal conductivity  $k$ , dynamic density, and bulk density  $q$ , all measured at a fixed pressure value. Notably, all thermophysical features were benchmarked using the Refprop 7.0 program. Moreover, the expression of the density and specific heat are used in the calculation according to (Span, et al., 1996). Additionally, considering the equations mentioned in (Span, et al., 1996), the density and specific heat were exhibited. Relation to the density and thermal conductivity were computed employing (Vesovic, et al., 1990).

The significant analyzing features of super-critical carbon dioxide and the effect of spacer on SHT which is the subject of current work were introduced in (Kim, et al., 2003 and Zahlan, et al., 2015). The

MHTC can improve supported by the flotation impact. The SC-CO<sub>2</sub> inflows in a vertically heated tiny pipe with an inner diameter of 2 mm scenario were examined experimentally by (Ruifeng P, et al., 2022). The experiment has been conducted using 7.5–9 MPa pressure, low ( $G < 200 \text{ kgm}^2\text{s}^{-1}$ )/high ( $G > 200 \text{ kgm}^2\text{s}^{-1}$ ) MF, and HF of 45–300 kWm<sup>2</sup>. Furthermore, the parameters of flotation force and inflow velocity were considered regarding the operation conditions. Although the high load capacity ( $q/G$ ), there was no indication of HT deterioration at low MFs, as reported as the result of such work.

The results of the work presented by (Zahlan, et al., 2015) revealed that heat transfer is continually enhanced and the coolant temperature was near its pseudo-critical mostly surpassing 100%. Furthermore, in the direction of panel separators, the heat transfer increased at up-flow meanwhile, the grid separator's effect of heat transfer was less prominent and mostly not shown at down-flow. Additionally, the authors utilized CFD identifications to expect influences on supercritical heat transfer. In this vein, the anticipations were noted to be appropriated with practical remarks, however, at doubtful accuracy for HTD conditions.

Before heat transfer, several procedures need to be considered at using SC-CO<sub>2</sub> in a cooling network besides energy circulation. The environmental harm technologies are now to be gradually eradicated and therefore alternative resources employing fluid refrigerants like carbon dioxide CO<sub>2</sub>. are acquiring additional attention, according to global agreements and European lawmaking.

Regarding these conditions, a significant deterioration in HT has been shown in cases of naked tubes and tubes equipped with obstacles. Also, considerable influences were recorded by changes in mass and HF's related to the supercritical heat transfer factor, however, it was not in terms of changes in inlet heat degree and pressure in line with the analysis of the parametric trends. Indeed, based on HTD conditions, it appears less dependent on MF under HTD. Such a fact is deemed as important reality in the bare tube investigations.

The authors (Xiao-jing, et al., 2022) examined a pipe with a diameter of 14.5 mm aiming to evaluate the heat transfer based on supercritical carbon dioxide in an upward direction. The pressure employed at the entrance ranged between 7.73 to 8.53 MPa while HF of

\* Corresponding author. Email: [ameer.a.jaddoa@uotechnology.edu.iq](mailto:ameer.a.jaddoa@uotechnology.edu.iq)

20.66 to 125.14 kW/m<sup>2</sup>, and MF of 393.7 to 940 kg/s (m<sup>3</sup>s). Also, several associations were estimated besides the flotation variables Bo and Bo\* throughout this experimental work. For the effect of flotation, it was used Bo while Nu used practical normalization. It was found that in Nu, all associations were generally identical. Further, the flotation effect appeared on heat transfer when Bo reached 104 with a temperature drop. However, when Bo-105 ( agrees with Jackson and Hall's limit).

To signify the HT demeanours controlling for flotation, a segmented association was considered. By relying on a dimensionless tube size together with criteria from various diameters, a universal benchmark was made, although the reality still needs extra empirical knowledge from different diameters to establish and enhance. The authors (Lei Wanga, et al., 2020) heated SC-CO<sub>2</sub> uniformly in horizontal circular smooth lines to study the nature of HT variations of the gas. The dimension of these tubes were inner diameters of 1.0 mm, 0.75 mm, and 0.5 mm. HT was shown that the HT was enhanced as a consequence of decreased critical point and that heat transmission.

The result illustrated that the HT indication was increased at a temperature close to a pseudo-critical level. Such an increase was attributed to turbulence brought on by the decline in fluidity besides the Prandtl number reaching the maximum level. Under these conditions, maximum thermal efficiency was achieved. However, the work tokened into account the outlet pressure, HF, MF, inlet heat degree, and tube diameter effects on heat transfer natural behaviour.

According to (Peng cheng, et al. ,2020), the expected S-heat CO<sub>2</sub>'s heat transfer is still questioned due to its complicity in terms of thermophysical priorities notply heating setting at high heat transfer related to MF ratios (q/G). Therefore, experimentally, the HT of S-CO<sub>2</sub> is studied in this mini pipe (d = 2 mm) on the scale of p = 7.6–8.4 MPa, q = 100–200 kW/m<sup>2</sup>, and G = 400–700 kg/m<sup>2</sup> s, with the proportion of q/G being within 250–500 J/kg. Thus, a discussion was introduced on the impact of these variables related to S-heat CO<sub>2</sub>'s transfer. In this context, these variables under constant circumstances appeared better performance in terms of input temperature, and a smaller diameter at a high MF value. Based on experimental demonstration, the local Nusselt number of SCCO<sub>2</sub> can be predicted over the inflow channel in which uniformly heated. Therefore, by taking into account both the flotation effect and changes in thermophysical characteristics, a novel heat transfer association for supercritical carbon dioxide with high q/G conditions is created. Besides that the heat transfer and inflow characteristics arise from SC-CO<sub>2</sub> which were studied by (Wenguang Lia, et al. 2022 ). The outcomes indicated a minor effect of pressure on heat transfer which has an opposite relationship with temperature and MF. Moreover, in all the models, the ratio of q/G harms heat transfer along with a robust flotation effect. Also, the association between SC-CO<sub>2</sub> with heat transfer were compared. The error reduction was strong mostly at pseudo-critical sites. More, using three-dimensional Reynolds-averaged Navier-Stokes methods the HX was investigated. This study was carried out employing the dynamics technique in ANSYS CFX counter-flow tube-in-tube.

On the other hand, utilizing single tube HX, the behaviour of SCO<sub>2</sub> inlet pressure, and wall heat transfer on supercritical carbon dioxide was analysed. After that, the identification of various parameters has been set out such as wall temperature in CFX-Post on MHTC based on the SST prototype. The research concluded that the practical average HT factor of supercritical carbon dioxide has extra precision compared to the other approaches.

The fluids SC-CO<sub>2</sub> need extra analysis through adopting novel methodologies on heat transfer behaviour to promote applications. In this vein, using mathematical analysis, the authors (Chao Lia, et al., 2022) introduced a model composed of three horizontal heat radiator pipes. The models were a straight tube, a converging pipe, and a diverging tube, aiming to analyse the heat transfer of supercritical liquid.

The outcomes compared with the homogeneous pipe model revealed that the homogeneous model has better performance and promotes heat transfer by 19.26% while the converging model reduced heat transfer efficiency. To make it clear, quasi-air film and eddy

blockage visions are presented to illustrate the degradation of heat transfer regarding the top edge. Also, eddy blockage gets worst and therefore leading to the degrading the heat transfer process at the top horizontal pipe by 17%. Similar outcomes were achieved related to the heat storage unit with (Ida et al.,2022, Kun et al.,2022, Hai et al.,2019; Scott Hai et al.,2022, and Wenlei et al.,2020).

To deal with restricting case of eddy blockage such criteria was proposed to modify the density and temperature of eddy blockage. Thus, one of the most interesting topics the heat transfer in refrigeration plumb inflows while accounting for the effects of flotation forces for heat pump systems, and air conditioners. Besides that to enrich the literature with the behaviour of heat transfer under various conditions. Accordingly, the aim here is to investigate these impediments related to supercritical heat transfer by justifying the thermal-hydraulic effect of fuel bundle spacers in SCWRS.

## 2. PROCEDURES OF APPROACH

The experimental of flowing at SCF pressure for restricted flow combined with calculating equipment is depicted in this part. Next, we present the analysis of HT through convection for the system illustrated in Figs. 1,2,3.



Fig. 1 Model under investigation

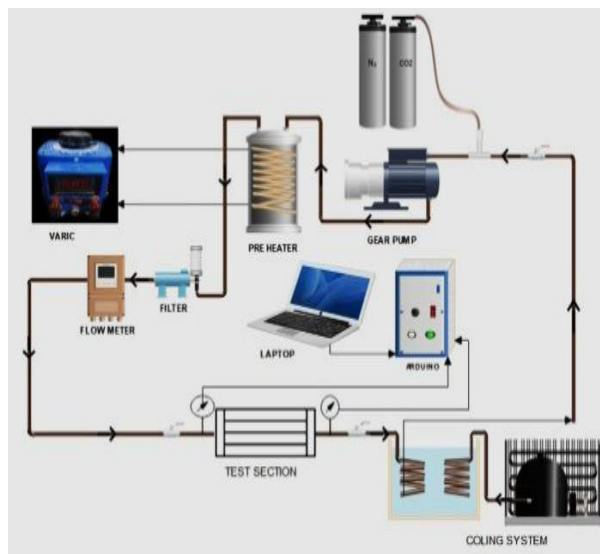
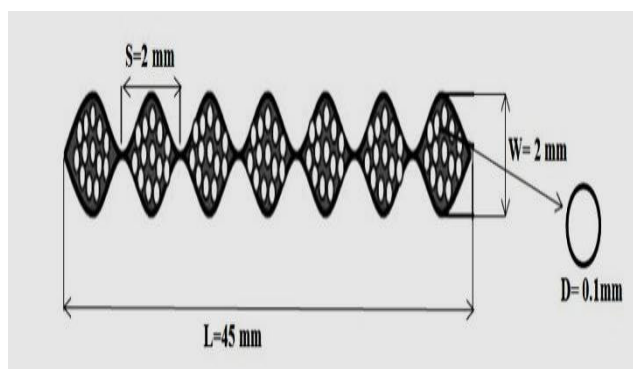


Fig. 2 Diagram of experimental model



**Fig. 3** Prototype Experimental Design of SC-CO<sub>2</sub>

The fluid parameters were driven by measuring the inlet and outlet mean temperature. The term (TR) (d) in this work is defined as the relationship between a single length of twist and a single length of the pitch (s) corresponding to the inner diameter of the pipe. The curved pipe is composed of curved pipes made of copper strips with 2 mm thick, 45 mm length, and 2 mm vast. According to the manual, the pipes were manufactured of copper material type 360. The dimensions are 0.5 cm in length and 0.8 cm in diameter. A compressing engine is normally used to push the gas 'ammonia' for cooling purposes. Figure 1(c) illustrates a pipe with an impediments pipe. it is worth mentioning that the purity of CO<sub>2</sub> used in this research was 99.7%. Experimentally, the system was run under continuous heat transfer cases.

The features of ethylene glycol gas represented by heat capacity control, and liquid properties at maximum-temperature stations give the reason why it is employed as a cooling gas. It is noteworthy that many coils were used for heat dissipation at the heating gas process and then under high pressure it converted to an ammonia solvent which became a dark blue solvent. In this regard, the pressured gas turn into amber under high temperature. Through a tiny hole, the ammonia fluid is then inflowed into the expansion valve. Noted that the pressure inside the hole is less than that of the outside of the hole, therefore, the ammonia fluid turns into gas at 27 degrees Fahrenheit leading to becoming pale blue due to evaporation. The most important component in the experimental system is the type of cooling unit since it could be broken in the case of re-heating.

The advantage of the components used in the test system is that all of them were made of stainless steel. Such a feature is importantly related to the handle's units since it prevents the steam from losing and getting out. Additionally, the path leaking can be identified using the double-sided weep apertures besides employing packing gland/body thread to resist the vibration. Moreover, to maintain the stem sturdy and versatile, a pair of two components were utilised. On the other hand, using Bourdon tube pressure gauge PG23HP-P the pressurize can be measured with a 1% precision (German manometers). In the same context, to evaluate a wide range of flow and document the flow average in bi-direction with a measurement precision of 2%. Further, a pair of thermal and pressurized sensors were utilized to adjust the intake regardless of the temperature or pressure. The object here is to guarantee the preciseness of the recording of the values, wherein the pressure can be dealt with up to 500 bar. In the case of breakdown, the device is covered to avoid uncontrolled. Noted that all other units are in a good condition and they work in a reliable situation under constant dynamic pressure. The flow recorder also has an estimation range of 0 to 30 L/min with an accuracy of 2%. The trigger pressurizes and heat level affects how precisely the totalizer records volume. An experiment was conducted using a data logger. The data recorder is a specific type of data processor that retains data as it is being captured and displays it instantly on the flow meter. The model under investigation can be captured the entire amount of benefits from integrated aggregates of units beside the sensor element's abilities based on absolute pressurize or temperature. To support the test model, a

detector type 5210-7 characterizes as a differential pressurizes wherein the aim here is to identify variation presser of inflows at the flow transcriber or throughout the channel.

This study serves as a prototype for evaluating CO<sub>2</sub> models because the procedures that were employed for precise measurement in this context included evaluating the CO<sub>2</sub> inflow rate besides the volume and pressure of the gas and saving and storing data. Four measurements of the flow of CO<sub>2</sub> may be seen simultaneously using a visual monitor and touchable. With flow measurement, the tool is quick to set up and use and measures immediately. The FLO-Sight program was set up and connected to the computer in order to manage the gas inflow meter. As a result, it shows that the options for showing the advanced data were selected. Another sensor used to measure heat levels is the Lm35 detector can sense the heat level precisely (mV). The Arduino Uno micro-controller was also used to control the heating activities. It is significant to note that the 10-bit storage range of 0 to 1023 and the input voltage range of 0 to 5 volts are inversely related to temperature variations. In the current work, the temperature will be commensurate to the voltage through Arduino (2 Celsius degrees Celsius) until it reaches the highest amount measured by the Lm35. The behavior of the prototype heat degree was examined using another temperature sensor, thermocouples type k, which was created at a time when metallurgical research was more advanced. Several sample properties may change because the temperature at which the sample was collected was between -200 and 1350 °C, or -330 and 2460 °F, in this instance. Further, type k thermocouples devices linked by a wire line depend on changes in semiconductor proprieties, also known as thermocouples. Additionally, the heat point is impacted by the thermoelectric effect, which depends on voltage and heat degree.

The thermocouple is one sort of heat detector that is often utilized. Thermocouples of type K also have a linear sensitivity of 41 V/°C and a chrome-aluminum construction. Upon temperature hit point of 185% (K-point) in the thermocouple sensor mean that the deflection reaches the Curie point. the CO<sub>2</sub> is removed using a filter housing (FH) made of carbon steel. One hundred bars of pressure cannot harm the FH. The high temperature could damage the test model, therefore it was employed Nichrome heating element. The fact of using such an element is that it fabricates 80% and 20% from nickel and chromium, respectively, consequently, keeping the cable out of damage. Additionally, it is oxidation-resistant and can coat itself in chromium oxide when heated. The Nichrome heating component is used as a bar with a length of 10 m, a current of 6.8 A, and an output of 1500 W. The supply voltage type (520T-10, Variac) was used with volt and current values of 10A and 130V, respectively.

There are three connection and output sockets on this device (110-volts-strong input power.). Because of the characteristic of cellulose represented by the ability of recyclable (75 to 85%), it is used as a thermal insulator beside it is a friendly environment. Boric acid and ammonium sulfate, which make up 15% of the remaining material, are fire retardants. Also, the method of manufacturing makes it non-flammable notably its compressed structure and non-toxic material.

The model of the current work was prepared from copper with a purity of 99.5%, and atomic weight. of 29. Also, the reason of adopted such a type is because of its strong thermal and electrical conductivity, ductility, and malleability. On its exposed surface, pure copper has a pinkish-orange colour. The production of electronics, tokens, naval hardware, and measurement equipment are just a few of the various sectors that use copper. This is mostly because it is an inexpensive material that is also added to different metal alloys to create jewelry like sterling silver, especially because it has the capacity to conduct heat and electricity.

### 3. DATA REDUCTION

The LMTD technique (Log Mean Temperature Difference) is typically used to estimate the total HT factor (H) over the entire length of each subsection that has been cooled down, as demonstrated below:

$$Q = LMTD \times H \times A \quad (1)$$

The below formula represents the average temperature logarithm of LMTD (opposite inflow):

$$LMTD = \left[ (T_{out,CO_2} - T_{in,water}) - (T_{in,CO_2} - T_{out,water}) \right] \times \ln \left( \frac{T_{out,CO_2} - T_{in,water}}{T_{in,CO_2} - T_{out,water}} \right)^{-1} \quad (2)$$

It is well known that there is an opposite relationship between water and carbon dioxide in terms of temperature and its behaviour various nonlinear with convection and distance from the model's input. Thus, the conventional logarithmic mean rate equation was chosen over an integral method proposed by (Ngo, et al., 2007 and Bruch, et al., 2009 ). To describe the average interior heat between carbon dioxide-DF and water at room temperature tiny piece of the exchange surface of the model is used as

$$DQ = H \times (T_{water} - T_{CO_2})DF \quad (3)$$

Note that the symbol U is used to indicate the general heat transfer. Also, the total heat transfer value over the experimental test gives the expression as

$$H = \frac{1}{F} \times \int_0^F \frac{DQ}{T_{water}DQ - T_{CO_2}DQ} = \frac{1}{F} \times \int_0^F H DF \quad (4)$$

Since heat degree variances on the water side were less than 3 OC, an approximately constant water heat degree along the test length was attained for all empirical settings:

$$T_{water}DQ^{-1} = T_{water} \quad (5)$$

The following formula is produced by the fluctuating temperature of the infinitesimal zone dS.

$$DF = \varepsilon (dh)_{CO_2} \quad (6)$$

The symbol (h) referred to supercritical carbon dioxide enthalpy. It can be noted that equations 4 to 6 can be represented the total heat transfer parameter to all sizes the test model.

$$H = \frac{\varepsilon}{F} \int_{h_{in}}^{h_{out}} (T_{water} - T_{CO_2})^{-1} dh \quad (7)$$

From the overall HT factor, the HT factor on the carbon dioxide side is calculated as follows:

$$\frac{1}{H} = \frac{1}{\alpha_{CO_2}} + \ln \frac{d_{ext}}{d_{in}} \times \frac{F_{exchange,internal}}{2\pi l \beta_x} + \frac{F_{exchange,internal}}{F_{exchange,external} \times \alpha_{water}} \quad (8)$$

As previously mentioned, for all models under examination, divergences in cooling water heat degrees were often smaller than 3 C, allowing us to assume that the water feature remained stable for the entirety of the trial. The value derived using the common LMTD approach was compared to the integral technique-based Carbon dioxide side HT factor for upward inflows in Figure 4. While the same pattern is observed in descending flows. For all pressures, the pseudo-critical temperature  $T_{pc}$  is where the main differences between the integral and LMTD techniques are focused, and as pressure increases, these differences become less important. These findings are related to the interaction between variations in heat degree and pressure and the specific heat  $C_p$  of supercritical CO2. The amount of  $C_p$  peaks at pseudo-critical temperature  $T_{pc}$ , and as pressure increases, the size of this crest decreases.

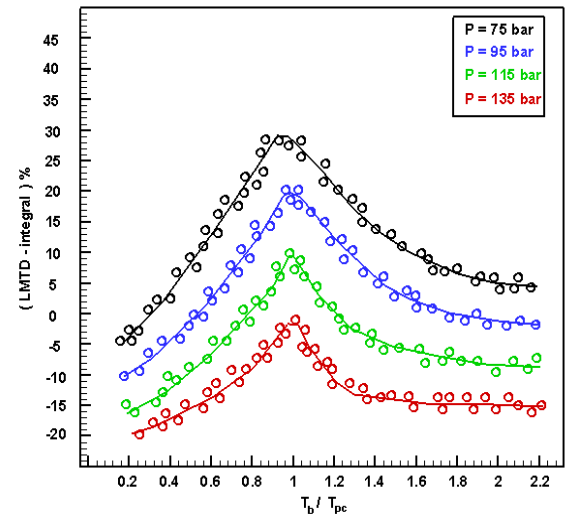


**Fig.4** Relation between LMTD and integral approach based on various pressures and upward flows.

With the aid of Figure 5, it can be noted that the variation in heat transfer achieved by this work utilizing two methods applied with different pressure values and with MF of  $G = 750 \text{ kg/m}^2 \text{ s}$ . Further, it can be remarked that there is a difference at 75 bars and 95 bars close to  $T_{pc}$ , however, these variations not appear in the fluid or gas-like regions. Additionally, the choice of the data deduction technique does not cause substantial variations across the entire temperature range between 115 bar and 135 bar and 135 bar.

Moreover, in normal conditions, the variation is 3%, and 7% outside of the pseudo-critical temperature  $T_{pc}$  and inside the pseudo-critical region, respectively, between the integral and LMTD approaches. Additionally, the CO2 along the test section only experienced tiny heat degree changes (less than 3 °C) when the mass heat degree was close to  $T_{pc}$ , however larger variations were seen when the mass heat degree was far from the pseudo-critical temperature (greater than 6-7 °C).

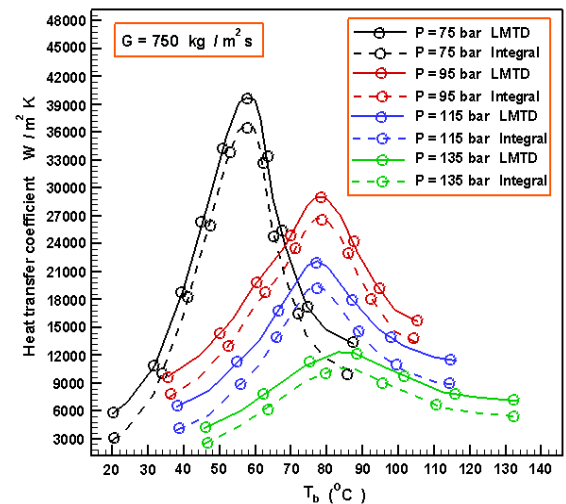


**Fig.5** For downward inflows, the differences between integral and LMTD approach.

An uncertainty analysis revealed that the HT factor's precision was frequently less than 20%. The typical uncertainty at 115 bars of pressure is shown in Figure 6. For ease of reading, uncertainties are not displayed in the remaining figures.

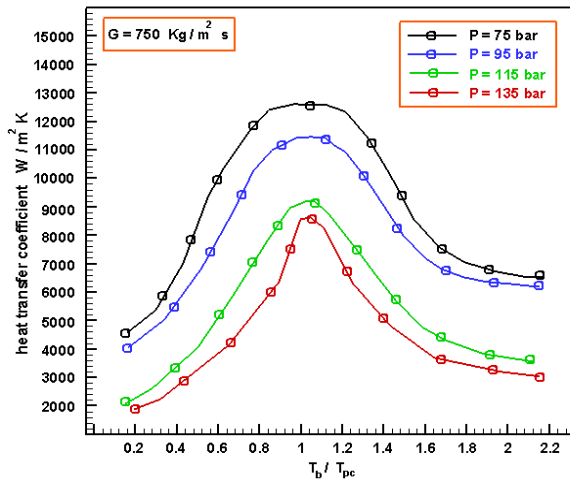


**Fig. 6** As a dimensionless temperature ( $T_b/T_{pc}$ ), the pressure behaviour due to HT coefficients is illustrated.

#### 4. RESULTS AND DISCUSSION

Measurements were made by meticulously examining the effects of the different process variables (pressure, input temperature, MF average, and inflow direction) on the HT factor.

##### 4.1 Operating pressure and its impact

Using parameters MF with  $G = 750 \text{ Kg/m}^2 \text{ s}$ , pressures (75 to 135 bars), downhill flows, the behavior of working pressures of heat transfer of  $\text{CO}_2$ . Similar phenomena are present with upward inflows but were not mentioned in this case. To represent the HT factor, two different feature temperatures are employed: I the mass liquid temperature on average, which is represented in  $T_b$  Figure 5 and equal to:

$$T_b = \frac{(T_{out} + T_{in})_{\text{CO}_2}}{2} \quad (9)$$

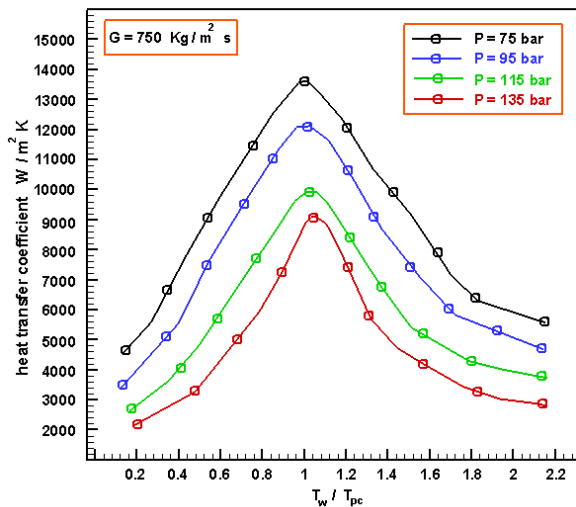


**Fig. 7** Using the dimensionless temperature  $T_w/T_{pc}$ ,  $T_w$ ,  $T_w$  to signify the pressure variation due to heat transfer coefficient in terms of wall temperature, upward flow.

(ii) For computing the average wall heat degree, the next formula is used in terms of average mass water heat temperature and heat transfer factor of water.

$$T_{w,int} = \frac{Q}{F a_{water}} + \frac{Q \ln \left( \frac{d_{ext}}{d_{in}} \right)}{2\pi l \beta_x} + T_{b,water} \quad (10)$$

Scientifically, for pressure, the heat transfer of gas and liquid regions is assumed to be constant. the top areas near pseudo-critical temperature which has high pressure the HT declined in this method. Therefore, such features are linked to the variation of heat degree and pressure. Furthermore, the direct relationship between pressure and the closer the pseudo-critical temperature, consequently, the smaller the heat transfer at low heat transfer parameter. Moreover, around the pseudo-critical temperature  $T_{pc}$ , the heat transfer factors are concentrated, this occurs upon using the mass fluid temperature  $T_b$ . Overall, according to the results, in presence of the dispersion of temperature, the most suitable choice to for modeling changes in the HT factor is mass liquid temperature  $T_b$ .

##### 4.2 Mass flux and its impact

The effect of the MF on the HT factor is depicted in Figures 8 and 9 for uphill and downward inflows, respectively, at a working pressure of 100 bars.

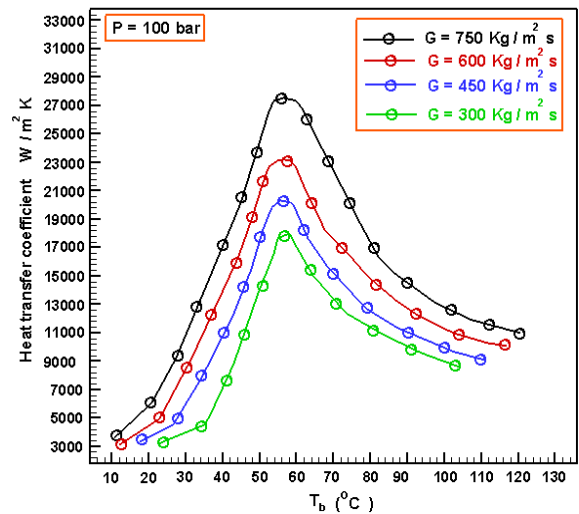


**Fig. 8** Upward flow scenario, mass flux behaviour in presence of heat transfer factor effect.

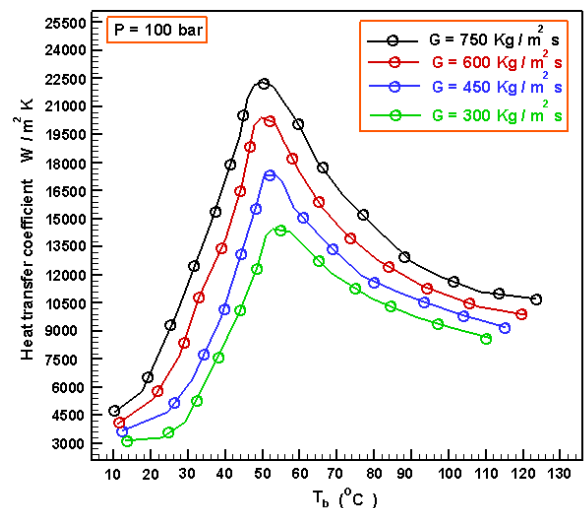


**Fig. 9** Behavior of mass flux and downward flow effected by heat transfer coefficient

As in the case of a liquid inflow with constant characteristics, an increase in  $G$  causes turbulent diffusion, which increases the HT factor of CO<sub>2</sub> for upward inflows. Downhill inflows exhibit various characteristics as determined by temperature and the MF average. This leads to a traditional tendency where the heat transfer coefficient for  $T_b T_{pc}$  lowers as MF decreases. The HT factor for  $T_b T_{pc}$  decreases as the MF average decreases from 750 Kg/m<sup>2</sup> s to 450 Kg/m<sup>2</sup> s. In reaction to further reductions, the MF rate rises, raising the HT factor. This distinct pattern, which is absent in upward inflows, demonstrates how free convection alters the temperature regime in a different way.

### 4.3 Inflow method and compound convection impact

For constant values of MFs of  $G = 490 \text{ kg/m}^2\text{s}$  and  $G = 750 \text{ kg/m}^2\text{s}$ , respectively, as well as for variations in mass liquid heat degree  $T_b$  and for different working pressures, Figures 10 and 11 illustrate the typical expression of the local HT factor. Upward and downward inflows were considered for each pressure and MF value and compared.

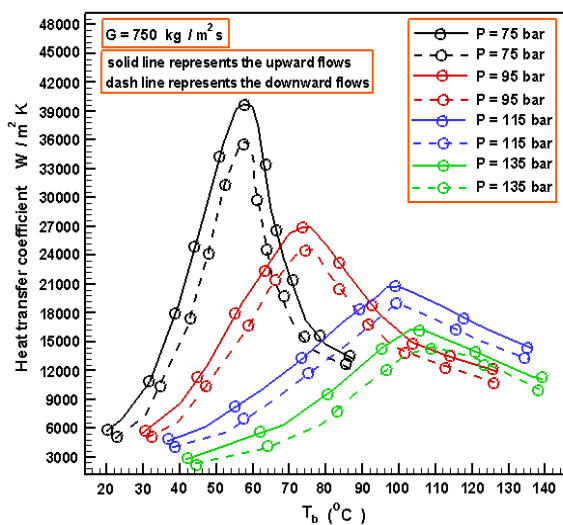


**Fig. 10** Comparison of heat transfer coefficient for downward and upward flows.

In the zone that resembles gas and is purely dependent on MF velocity, the HT factor reaches its highest value. This shows that forced convection is the main means of heat transfer. However, due to the lack of data at temperatures greater than 120 °C, it is impossible to draw a definite conclusion regarding the effect of inflow direction on the HT factor. Considerable changes in inflow direction are shown for all bulk flows in the pseudo-critical zone, indicating a significant contribution of buoyant forces to heat transfer. Similar patterns are displayed in the fluid-like zone, with the exception of the maximum bulk input rate.

The beginning of mixed heat load is connected to the radial density gradient. The HT factor improves in upward inflow and deteriorates in downward inflow when composite heat load occurs, according to research on opposing and encouraging turbulent composite heat load, respectively. These theories are validated using a mixed heat load variable. The source of the Richardson number is:

$$\text{Richardson number } Ri = Gr Re^{-2} \quad (11)$$

The buoyancy forces and inertial forces can be contrasted using such a numerical number. The semi-empirical variable, with a format similar to the Richardson number, was developed by Hall and Jackson (J.D. Jackson, et al. 1979) to explain the effects of natural heat load on turbulent plumb inputs of heated SC-CO<sub>2</sub>. When it comes to this variable, mixed heat load has a big impact on heat transfer when:

$$Gr Re^{-2.7} > 10^{-5} \quad (12)$$

The Reynolds number can be calculated using the integral format as

$$Re = [D_h G \times (h_{out} - h_{in})^{-1}] \times \int_{h_{in}}^{h_{out}} \frac{dh}{\mu h} = G \times D_h \times \mu_b^{-1} \quad (13)$$

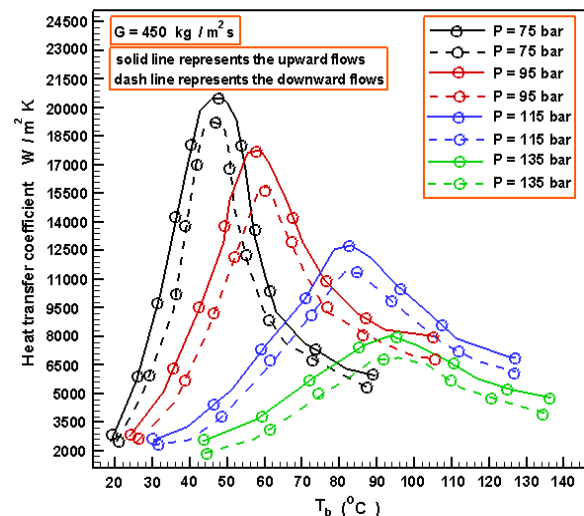


**Fig. 11** For downward and upward inflows, the variation of heat transfer coefficient is shown.

While Grashof number  $Gr$  was computed using the following expression:

$$Gr = \rho_b^2 D^3 g - \rho_{ave} \rho_b D^3 g (\mu_b^2)^{-1} \quad (14)$$

Using the expression in (Bae, et al., 2005) besides expression 14 (adopting the argument between the mass density and the standard density), the effect of the radial density gradient can be expressed as in eq. 15. Such factor mainly ignites buoyant inflows.

$$\rho_{ave} = \frac{\rho_w + \rho_b}{2} \text{ if } T_w > T_{pc} \text{ or } T_b < T_{pc}$$

$$\rho_{ave} = \frac{\rho_b T_b - \rho_b T_{pc}}{T_b - T_w} \text{ if } T_w < T_{pc} < T_b \quad (15)$$

Under various pressure values (14), using dimensionless temperature ( $T_b/T_{pc}$ ) starting from high to low MF, figures (12) and (13) illustrate the elevation of the mixed convection factors. As introduced in (Jackson, et al., 1979), the boundary value of the combined convection factors regarding the impact of buoyant forces under heating conditions is shown in Figure 10. Since all of the upward and downward inflows are identical, the downhill inflows data were depicted. Here, it must be confirmed that the outcomes presented in figures 8 and 9 are reliable, besides that it should focus on the convection and its effect at the pseudo-critical site for fully taken-in MFs. In this context, in the fluid-like zone, the HT at moderate to low MFs the convection is a significant effect at the top MFs region. Thus, at the gas-like region, to heat entire MFs forced convection was utilized. For more evidence, experimentally, at  $G = 300 \text{ Kg / m}^2\text{s}$ , the effect of the mixed convection is influential using a temperature scale. This value is consistency with the results found in (J.D. Jackson, et al., 1979).

Figure 15 presents the results in a dimensionless style that is widely used in studies on composite heat load under hot conditions. Additionally, a Nusselt value obtained from a pure forced heat load relationship is used to reduce the empirical Nusselt value and it is exhibited in accordance of the composite heat-load value that was described earlier.

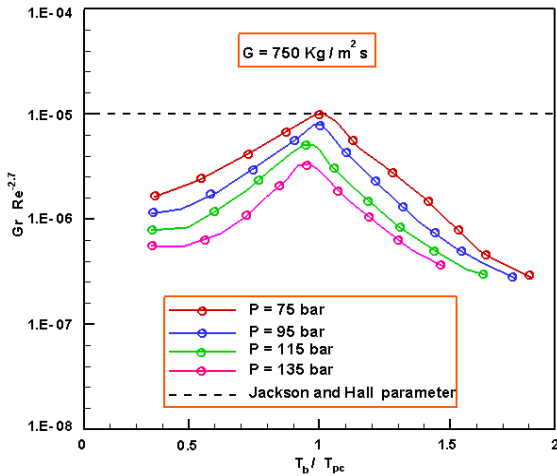


**Fig. 12** In terms of dimensionless temperature, the compound convection factor ( $T_b/T_{pc}$ ) at  $G = 750 \text{ Kg / m}^2 \text{ s}$ .

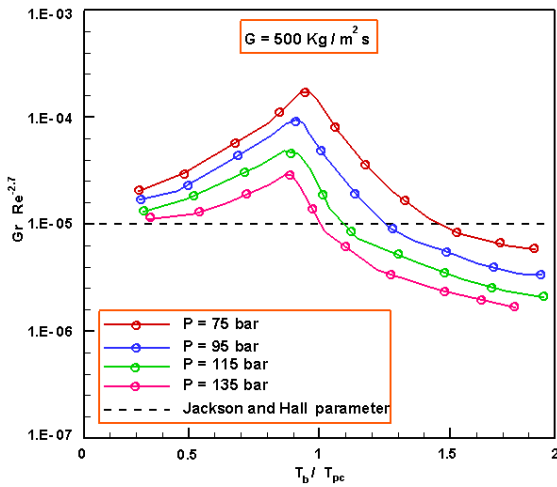


**Fig.13:** In terms of dimensionless temperature, the compound convection factor ( $T_b/T_{pc}$ ) at  $G = 500 \text{ Kg / m}^2 \text{ s}$

According to ( Jackson, et al., 1979), the Krasnoshchekov relationship has been chosen for pure forced heat load relationships.

$$Nu_{\text{forced convection}} = 0.0183 Pr_b^{0.5} Re_b^{0.82} \left(\frac{\rho_b}{\rho_w}\right)^{-0.3} \quad (16)$$

The mean average heat integrated between the mass liquid heat degree and the wall heat point was used to get the Prandtl value, i.e.

$$C_{p \text{ average}} = (h_b - h_w) \times (T_b - T_w)^{-1} \quad (17)$$

and

$$\text{Prandtl number}_{\text{average}} = C_{p \text{ average}} (h_{\text{out}} - h_{\text{in}})^{-1} \times \int_{h_{\text{in}}}^{h_{\text{out}}} \frac{dh}{\omega h} \quad (18)$$

Single curves for uphill and downstream inflows were obtained when the Nusselt value was plotted in terms of the variable ( $Gr \times Re^{-2.7}$ ), respectively. Their geometries are similar to composite heat loads under heating conditions in this context. Figure 13 also illustrates three distinct thermal regimes, including forced convection, which is the primary method of heat transmission at low values of the composite heat load

parameter ( $Gr \times Re^{-2.7}$ ), free heat load, which has negligible impact, and  $Nu_{\text{exp}}/Nu_{\text{fc}}$ , which is roughly equal in all inflow directions. Furthermore, this demonstrates good concordance between the actual findings and the forced heat load relationship discovered in (J.D. Jackson ,et al., 1979).

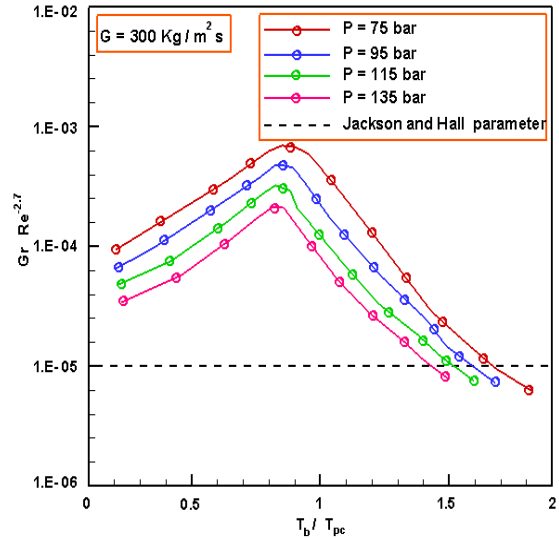


**Fig.14** In terms of dimensionless temperature, the compound convection factor ( $T_b/T_{pc}$ ) at  $G = 300 \text{ Kg / m}^2 \text{ s}$

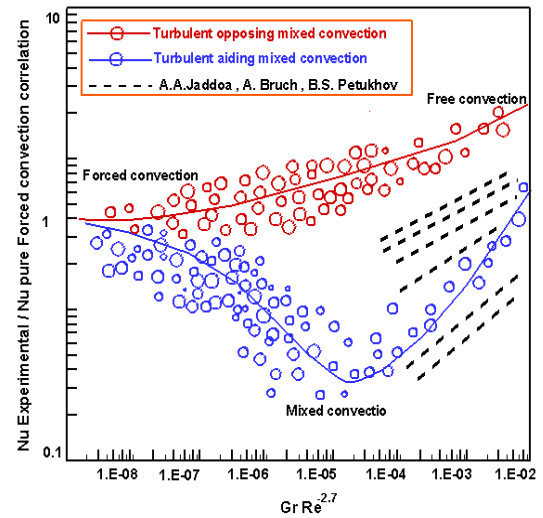


**Fig.15** Performance of mixed convection parameter related to Nusselt number.

When a result, floatation forces increase and variations in inflow direction are visible as the factor ( $Gr \times Re^{-2.7}$ ) grows. This backs up the observed and represented behaviors in Figures 8 and 9. Here, the heat transfer was exacerbated by descending inflows and improved by rising flows for different scenarios. Changes in velocity profiles and the consequent development of turbulence as a result of floatation forces can also be used to explain this. Relaminarization is the term for this behaviour in turbulent composite heat load (Aicher, et al. ,1997 and Fewster, et al., 1976). Additionally,  $Gr \times Re^{-2.7}$  has the most down HT factor values, which range from  $2.10^{-5}$  to  $4.10^{-5}$ . The greatest values of ( $Gr \times Re^{-2.7}$ ) favors-free heat load and practical HT are consistent with the useful rule designated for SC-CO<sub>2</sub> under heating conditions by (Petukhov, et al., 1964).This demeanour is referred to as "relaminarization" in unstable composite heat load (Aicher, et al., 1997 and Fewster, et al., 1976). Furthermore, the lowest HT factor amounts, spanning from  $2.10^{-5}$  to  $4.10^{-5}$ , are found for ( $Gr \times Re^{-2.7}$ ). Maximum

values of  $(Gr \times Re^{-2.7})$  favors-free heat load and empirical HT agrees well with the practical law established by ( Petukhov, et al., 1964) for SC-CO2 under heating states:

$$\frac{Nu_b}{Nu_{FC}} = 15 (Gr \times Re^{-2.7})^{0.4} \quad (19)$$

#### 4.4. Heat transfer and its predictive correlation relationship

The only fundamental contributions to the estimation of the HT factor of cooled SC-CO2 are correlations made for horizontal inputs. In these cases, simply (S.M. Liao et al 2002) used a relationship that took into account the Richardson value to account for the composite heat load's influence. The empirical findings were contrasted with six correlations (Jaddoa, 2021a,b,2022, Bruch, et al., 2009, and Son, et al., 2006) that were produced for SC-CO2 under cooling conditions. Figures 16 and 17 compare these projected techniques with our empirical results for a suitable MF rate of  $G = 300 \text{ kg/m}^2\text{s}$ , where a significant impact of floatation force was discovered. The empirical data and the forecasting models show significant differences for downhill inflows, especially in the fluid-like zone and the pseudo-critical region. These behaviors are thus linked to the rise in composite heat load and, in turn, to the deterioration of heat transport caused by the relaminarization phenomenon. The gas-like zone exhibits excellent agreement with the relationships developed by (A.A. Jaddoa, 2021a,b,2022, and Bruch et al., 2009). This shows that buoyant forces shouldn't influence inflow direction unless they have a significant impact. The relationship between (Jaddoa, a2021,b 2022 and Bruch et al., 2009) The empirical results and the simulation approaches differ significantly for downward inflows, especially in the fluid-like zone and the pseudo-critical region. The increase in composite heat load and, consequently, the deterioration of heat transport caused by the relaminarization phenomenon are related to these actions. The gas-like zone exhibits excellent agreement with the relationships developed by (Jaddoa, 2021a,b,2022, and Bruch et al., 2009). This shows that buoyant forces shouldn't influence inflow direction unless they have a significant impact. The connection between (Jaddoa, 2021a,b 2022 and Bruch et al., 2009).

The aforementioned correlations were developed for horizontal inflows. Therefore, additional correlations were proposed using the data on vertical turbulence's assistance and opposition to composite heat load under cooling conditions.

Using the (Jackson, et al., 1979) variable, the best fit to our empirical findings in turbulent assisted composite heat load yields:

$$Gr Re^{-2.7} < 5.3 \times 10^{-5} ; \frac{Nu_b}{Nu_{FC}} = 1 - 83 \times (Gr Re^{-2.7})^{0.38} \quad (20)$$

$$Gr Re^{-2.7} > 5.3 \times 10^{-5} ; \frac{Nu_b}{Nu_{FC}} = 1 - 23 \times (Gr Re^{-2.7})^{0.57} \quad (21)$$

The correlation between the turbulent opposing composite heat load and the SC-CO2 heating parameters was found by (J. Fewster in 1976). Additionally, the empirical results were fit while keeping the exponents of the correlation (Fewster 1976):

$$\frac{Nu_b}{Nu_{FC}} = [1.385 + 5634 (Gr Re^{-2.7})^{0.74}]^{\frac{1}{5}} \quad (22)$$

#### 4.5 The Resistance of the Flow

The friction element could be precisely predicted from empirical data for common liquids like water and air using the equation suggested by (Aerov and Tojcek 2006), as shown by (Earlier et al., 2006).

$$Fr_b = \frac{\varepsilon^3}{1-\varepsilon} \times \frac{\rho_f l_p}{3M^2} \times \frac{\Delta P}{L} = \left( \frac{60.435}{Re_b} \right) + 0.562 \quad (23)$$

where  $Re_b$  is the equivalent Reynolds number defined as:

$$Re_b = \frac{2Ml_p}{3\mu_f(1-\varepsilon)} \quad (24)$$

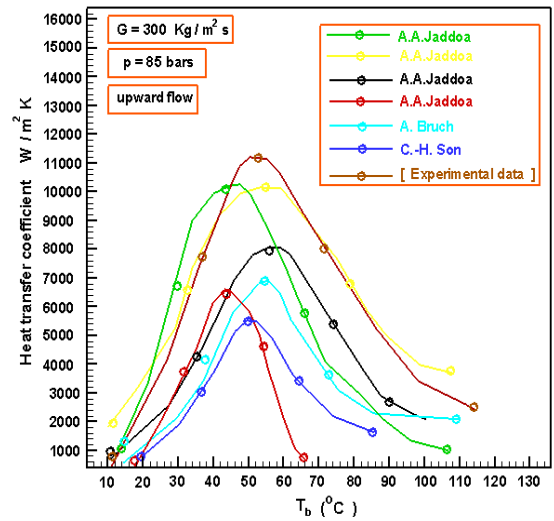


Fig.16 For downward flow scenario, difference correlations and its relation with heat transfer.

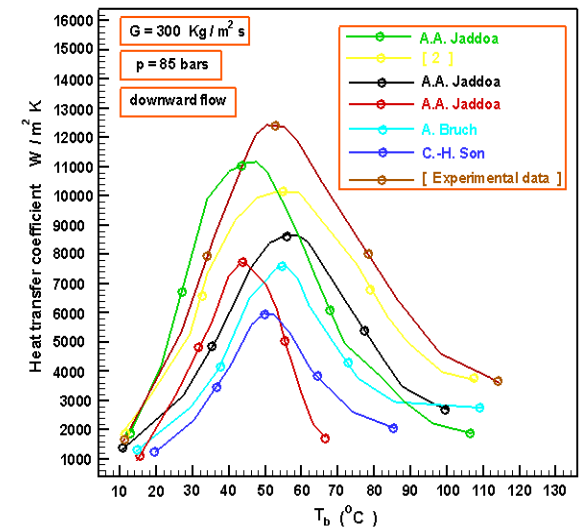


Fig. 17 For upward flow scenario, difference correlations and its relation with heat transfer.

The friction factor for carbon dioxide influx in sintered tubes at SC pressures is shown in Figures 18 and 19 and was calculated using empirical data. It was discovered that the carbon dioxide in sintered tubes friction factors at SC pressures and invariant heat (cold) closely match Formula 23. The friction factors for carbon dioxide flowing in heated sintered tubes at SC pressures, however, are significantly larger than those predicted by Formula 23 as illustrated in Figure 18. This means that the increased friction factors may be influenced by the different thermo-physical properties of the sintered tubes and the speed of the liquid flow. Two innovative relationships were developed using the experiment results and the thermal performance of CO2 to calculate friction factors in heated sintered tubes.

$$Fr_b = \left( \frac{98.687}{Re_b} \right) + 0.754 \quad (25)$$

The values of  $Re_b$  was given as:

$$Re_b = Re_b^* \left( \frac{\mu_w}{\mu_f} \right)^n \left( \frac{\rho_w}{\rho_f} \right)^m \quad (26)$$

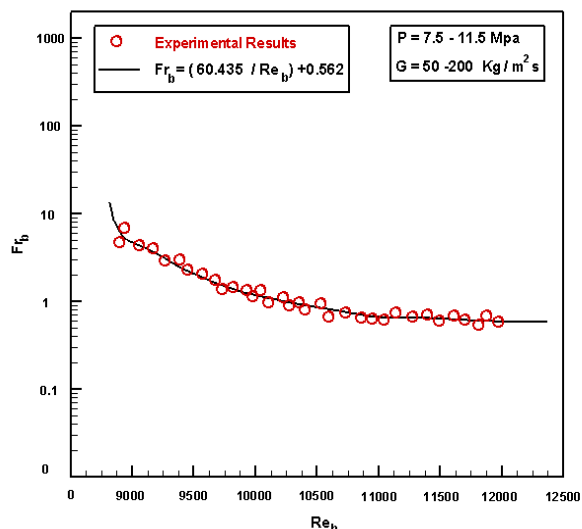


**Fig.18.** Friction characteristic for carbon dioxide at SC pressures in the sintered channels (cold case):  $p = 7.5\text{--}11.5\text{ MPa}$ ,  $G = 50\text{--}200\text{ kg/m}^2$

Due to the dispersion of empirical results across the damaged area, about 18% accuracy was gained by aiding compound convection vs compound convection. Wherein about 80% of 420 were to be predicted within the 13% accuracy restrictions.

Information dispersion in turbulent composite heat loads that promote heating has also been observed frequently in empirical (Jackson et al. 1979, Fewster et al., 1976) and computational (Bae et al., 2005) research. This dispersion may be caused by instability during the relaminarization phenomenon.

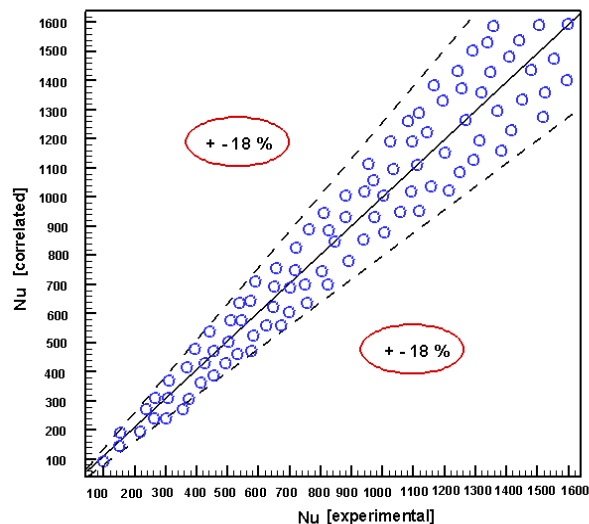


**Fig. 20** Downward flow scenario, experimental results vs. suggested correlation.

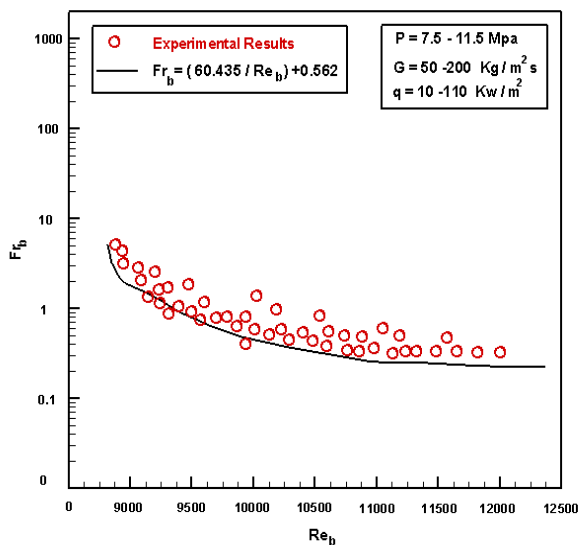


**Fig.19.** Friction characteristic for carbon dioxide at SC pressures, heating sintered channels:  $p = 7.5\text{--}11.5\text{ MPa}$ ,  $G = 50\text{--}200\text{ kg/m}^2\text{ s}$ ,  $q = 10\text{--}110\text{ Kw/m}^2$

$Re_b$  considers the effects of differential mass and viscosity in this work, where ( $f$  and  $f$ ) are the density and viscosity according to main averages of the inside and outside heat points and pressures and ( $n = 4.63$ ,  $m = 2.33$ ) for inflow.  $w$  and  $w$  represent the mass and viscosity averages relying on the inside main heats of the wall and pressures. Equation 23 and Figure 22 next to each other show how well Equation 23 predicts the friction factor compared to Equation 24. Due to the influence of buoyancy and various thermo-physical features, the inflow impedance for inflow depressed value is higher than that of upward inflow direction in this situation.

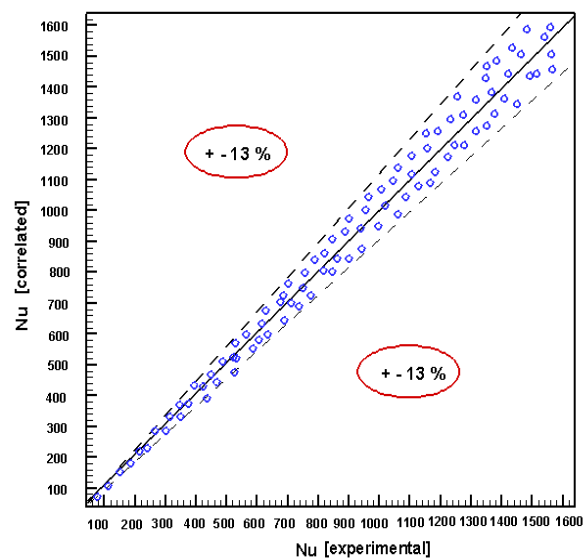


**Fig. 21.** Upward flow scenario, experimental results vs. suggested correlation.

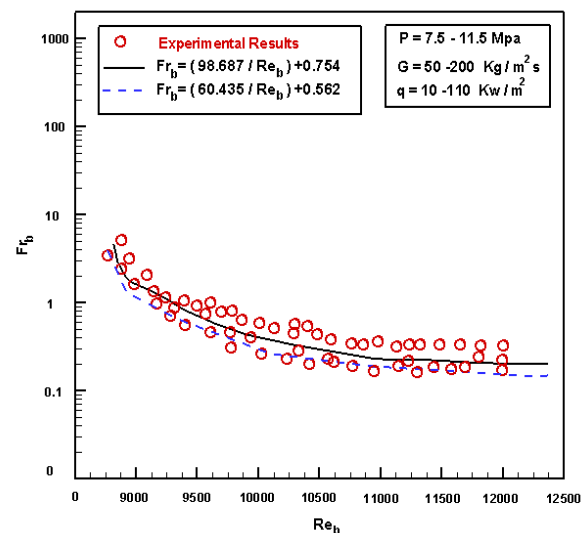


**Fig. 22.** Relationships for the friction characteristic for carbon dioxide at SC pressures, heating sintered channels scenario :  $p = 7.5\text{--}11.5\text{ MPa}$ ,  $G = 50\text{--}200\text{ kg/m}^2\text{ s}$ ,  $q = 10\text{--}110\text{ Kw/m}^2$ .

## 5 CONCLUSIONS

Empirical investigation was conducted to look at HT during the cooling of turbulent SC-CO<sub>2</sub> upward influx. The HT factors were identified using specific data reduction techniques, and the effects of system variables like pressure, MF, and input direction on the HT process were investigated. Major observations are summarized in the following:

1. The HT factor peaks as the mass temperature approaches the pseudo-critical heat degree  $T_{pc}$ , while the maximum value decreases as pressure increases. Additionally, neither the fluid-like nor gas-like zones had any observable effects of pressure on the HT factor. The specific heat changes similarly with pressure and temperature, which means that these behaviors are related to those changes.
2. The HT component in upward inflows increases in response to an increase in MF. The creation of composite heat load may be the explanation for the empirically discovered MF velocity threshold below which a reduction raises the HT factor in downhill inflows.
3. When comparing the HT factor for uphill and downhill inflow directly, it is possible to observe the influence of inflow direction and, consequently, buoyant forces. Particularly in the fluid-like and pseudo-critical regions was such an effect visible. Additionally, a potential effect of the free heat load might be noticed in the gas-like zone for the lowest values of MF velocity.
4. To look at composite heat load, an approach identical to that utilized in the experiments under heating conditions was used. It was particularly examined how the effect of composite heat load might be affected using the composite heat load factor and criterion established by (J. Fewster 1976).
5. Good agreement between cooling data and actual findings was observed. With the help of the dimensionless composite heat load factor, the Nusselt value was also visualized. Furthermore, a single curve was produced for both turbulent composite heat loads that were opposing and supporting each other. This demonstrates that the thermal behavior of the composite heat load matched that of heating and cooling conditions, and it also demonstrates that the information could be condensed using the chosen dimensionless band. The new results close the knowledge gaps in the earlier works on turbulent vertical composite heat load under cooling conditions.
6. Using two unique correlations, the friction factors of SC-CO<sub>2</sub> in heated porous restricted flow were predicted. The suggested procedures generated precise results that were comparable to those attained by experiments carried out as part of the ongoing investigation.
7. Finally, specific connections were developed with a precision of 13% and 18%, respectively, for upward and downward inflows.

## ACKNOWLEDGEMENTS

This research was supported by the University of Technology – Iraq

## NOMENCLATURE

$C_p$	Specific heat, J/Kg K
$D$	Diameter of tube, m
$s$	Length of twisted tape, m

$Q$	flow rate, W
$m$	mass flow rate, kg/s
$Nu$	Nusselt number
$A$	area, m <sup>2</sup>
$T$	Temperature, K
$G$	mass flux, kg/m <sup>2</sup> s
$g$	gravity of acceleration, m <sup>2</sup> /s
$Gr$	Grashof number
$U$	coefficient of overall heat transfer, W/m <sup>2</sup> K
$Pr$	Prandtl number
$Ri$	Richardson number
$h$	specific enthalpy, J/kg
$H$	coefficient of heat transfer, W/m <sup>2</sup> K

### Greek symbol

$\alpha$	coefficient of heat transfer, W/m <sup>2</sup> K
$\beta$	conductivity of thermal, W/m <sup>2</sup> K
$\mu$	dynamic viscosity, Pas
$\rho$	Density, Kg/m <sup>3</sup>

### Subscript and superscript

w	water
h	hydraulic
b	bulk
in	inlet
out	outlet
pc	pseudo-critical
ext	external
exp	experimental data
Fc	Force and free convection

## REFERENCES

- A.A. Jaddoa, 2021, "Convection Heat Transfer Performance For The SCf-CO<sub>2</sub> Media In Mini-Tube With Fins Experimentally" *Journal of Engineering Science and Technology*, 16(4), 3407 – 3420.  
<https://jestec.taylors.edu.my/Vol%2016%20Issue%2>
- A.A. Jaddoa, 2021, "Convection Heat Transfer Analysis with Flow Resistance for Mini-Helically Coiled Tubes at Supercritical Pressures Experimentally", *International Journal of Heat and Technology*, 39(3), 817-824.  
<https://doi.org/10.18280/ijht.390315>
- A. A. Jaddoa, 2022, "Experimental investigation of supercritical fluid heat transfer properties in a miniature heat sink", *Journal of Mechanical Engineering*, 19(2), 41-63.  
<https://ir.uitm.edu.my/60647/1/60647.pdf>
- A. Bruch, A. Bontemps, S. Colasson, 2009, "Experimental investigation of heat transfer of supercritical carbon dioxide flowing in a cooled vertical tube", *International Journal of Heat and Mass Transfer*, 52, 2589–2598.  
<https://doi.org/10.1016/j.ijheatmasstransfer.2008.12.021>
- Ahmad Eter, Dé Groeneveld, , Stavros Tavoularis, 2017, "Convective heat transfer in supercritical flows of CO<sub>2</sub> in tubes with and without flow obstacles", *Nuclear Engineering and Design*, 313, 162–176.  
<https://doi.org/10.1016/j.nucengdes.2016.12.016>
- B. J. Kkilefa, A.A. Jaddoa, and A. H. Reja, 2021, "Experimental investigation of heat transfer features for vertical tube using porous media and Carbon dioxide", *Journal of Mechanical Engineering Research and Developments*, 44 ( 5 ), 188-195.  
<https://scholar.google.com/citations?>

B.S. Petukhov, L.I. Roizen,1964,” Generalized relationships for heat transfer in a turbulent flow of a gas in tubes of annular section”, *High Temp.* ,2 , 65–68.

<http://mi.mathnet.ru/tvt871>

C.-H. Son, S.-J. Park,2006, “ An experimental study on heat transfer and pressure drop characteristics of carbon dioxide during gas cooling process in a horizontal tube” , *Int. J. Refrig.* ,29 (4) , 539–546.

<http://10.1016/j.ijrefrig.2005.10.010>

Chao Lia, Junhon gHaoa ,Xingce Wang , Zhihua Gea ,and Xiaozhe Dua, 2022, “Dual-effect evaluation of heat transfer deterioration of supercritical carbon dioxide in variable cross-section horizontal tubes under heating conditions”, *International Journal of Heat and Mass Transfer*, 183, Part A, 122103.

<https://doi.org/10.1016/j.ijheatmasstransfer.2021.122103>

Eter, A., Groeneveld, D., Tavoularis, S., 2016, “An experimental investigation of supercritical heat transfer in a three-rod bundle equipped with wire-wrap and grid spacers and cooled by carbon dioxide” , *Nucl. Eng. Des.* ,303, 173–191.

<https://doi.org/10.1016/j.nucengdes.2016.04.002>

G. Lorentzen, 1995,”The use on natural refrigerants: a complete solution to the CFC/ HCFC predicaments”, *Int. J. Refrig.* 18 (3) , 190–197.

[https://doi.org/10.1016/0140-7007\(94\)00001-E](https://doi.org/10.1016/0140-7007(94)00001-E)

Hai-Dong Wang, Zeng-Yuan Guoa,2019,” physical heat transfer” *Frontiers in Heat and Mass Transfer*,13(2),1-12,

[https:// DOI: 10.5098/hmt.13.20](https://doi.org/10.5098/hmt.13.20)

Ida Bagus Alit, I Gede Bawa Susana, I Made Mara,2022,” thermal study of the dryer with heat exchanger pipe installed in rice husk double furnace during drying white turmeric”, *Frontiers in Heat and Mass Transfer*, 19(25),1-7.

[https:// DOI: 10.5098/hmt.19.25](https://doi.org/10.5098/hmt.19.25)

J.D. Jackson, W.B. Hall, 1979, “Influences of buoyancy on heat transfer to fluids in vertical tubes under turbulent conditions”, in: *S. Kakaç, D.B. Spalding (Eds.), Turbulent Forced Convection in Channels and Bundles, Hemisphere, New York.*

[https://doi.org/10.1016/S0017-9310\(97\)00026-4](https://doi.org/10.1016/S0017-9310(97)00026-4)

J.D. Jackson, W.B. Hall,1979,” Forced convection heat transfer to fluids at supercritical pressures, in: *Turbulent Forced Convection in Channels and Bundles*, *Hemisphere* New York, 2,563–611.

[https://doi.org/13.1044/6.678923](https://doi.org/10.1016/0017-9310(97)00026-4)

J.H. Bae, J.Y. Yoo,1964,” Direct numerical simulation of turbulent supercritical flows with heat transfer” , *Phys. fluids* ,17 , 1–24.

<https://doi.org/10.1063/1.2047588>

J. Fewster,1976,” Mixed convection and free convective heat transfer to supercritical pressure fluids flowing in vertical tubes”, Ph.D. *Thesis, University of Manchester.*

<https://ethos.bl.uk/OrderDetails.do?uin=uk.bl.ethos.524682>

Kun Zhang , Zhiyong Li a Jia Yao ,2022,” numerical study on heat transfer characteristics of corrugated tube phase change thermal energy storage unit”, *Frontiers in Heat and Mass Transfer*, 19(5),1-8.

[https:// DOI: 10.5098/hmt.19.5](https://doi.org/10.5098/hmt.19.5)

Lei Wang, Yu Cheng , Pana Jin Der, Leeb YanWang , and Ben-Ran Fud Chin Pane, 2020, “Experimental investigation in the local heat transfer of supercritical carbon dioxide in the uniformly heated horizontal miniature tubes” , *International Journal of Heat and Mass Transfer*, 159, 120136.

<https://doi.org/10.1016/j.ijheatmasstransfer.2020.120136>

M.H. Kim, J. Pettersen, C.W. Bullard,2003, “Fundamentals process and system design issues in CO2 vapor compression systems” , *Process Energy Combust. Sci.* ,30 , 119–174.

<https://doi.org/10.1016/j.peccs.2003.09.002>

Peng cheng ,Gu oShou ,chun Liu ,Jianguo Yan Junhui and Wang Qiao ling Zhang,2020, “ Experimental study on heat transfer of supercritical CO2 flowing in a mini tube under heating conditions”, *International Journal of Heat and Mass Transfer*, 153, 119623.

<https://doi.org/10.1016/j.ijheatmasstransfer.2020.119623>

R. Span, W. Wagner, 1996 , “A new equation of state for CO2 covering the fluid region from the triple-point temperature to 1100 K at pressures up to 800 MPa”, *J. Phys. Chem.* , 25 (6) , 1509–1596.

<https://doi.org/10.1063/1.555991>

Ruifeng Penga ,Xi anliang Leia , Ziman Guoa Yahu, Wang Hu , and ixiong Lia XuZ houb,2022, “Forced convective heat transfer of supercritical carbon dioxide in mini-channel under low mass fluxes”, *International Journal of Heat and Mass Transfer*, 182, 121919.

<https://doi.org/10.1016/j.ijheatmasstransfer.2021.121919>

Scott Wahlquist , Amir Ali a, Su-Jong Yoon , Piyush Sabharwall,2022,” laminar flow heat transfer in helical oval-twistedtube for heat exchanger applications” *Frontiers in Heat and Mass Transfer*,18(35),1-8,

[https:// DOI: 10.5098/hmt.18.35](https://doi.org/10.5098/hmt.18.35)

S.M. Liao, T.S. Zhao,2003, “ Measurements of heat transfer coefficients from supercritical carbon dioxide flowing in horizontal mini/micro channels”, *J. Heat Transfer* ,124 , 413–420.

<https://doi.org/10.1115/1.1423906>

T. Aicher, H. Martin, 1997,”New correlations for mixed turbulent natural and forced convection heat transfer in vertical tubes”, *Int. J. Heat Mass Transfer* ,40 (15) ,3617–3626.

[https://doi.org/10.1016/S0017-9310\(97\)00026-4](https://doi.org/10.1016/S0017-9310(97)00026-4)

T.L. Ngo, Y. Kato, K. Nikitin, T. Ishizuka, M. Utamura, 2007, “Empirical correlations for heat transfer and pressure drop in a new microchannel hot water supplier” , in: *Proceedings of the Heat Set conference, Chambery, France*, 411–420.

<https://www.researchgate.net/publication/335501157>

V. Vesovic, W.A. Wakeham,1990, “The transport properties of carbon dioxide”, *J. Phys. Chem.* , 19 (3) ,1509–1596.

<https://doi.org/10.1063/1.555875>

Wenguang Lia, Zhibin Yua, Yi Wang, Yongliang Li,2022, “ Heat transfer of supercritical carbon dioxide in a tube-in-tube heat exchanger-a CFD study” , *The Journal of Supercritical Fluids*, 181, 105493.

<https://doi.org/10.1016/j.supflu.2021.105493>

Wenlei Lian, Zijian Sun, Taoyi Han and Yimin Xuan,2020,” experiment study on the boiling heat transfer of liquid film in a rotating pipe”, *Frontiers in Heat and Mass Transfer*,14(10),1-6,

[https:// DOI: 10.5098/hmt.14.10](https://doi.org/10.5098/hmt.14.10)

Xiao-jing Zhua , Rui-zeng Zhanga , Xin Dua , XiaoYub , and Qing-gangQiu 2022 , “Experimental study on heat transfer deterioration of supercritical CO2 in a round tube:A boundary assessment” , *International Communications in Heat and Mass Transfer*, 134, 106055.

<https://doi.org/10.1016/j.icheatmasstransfer.2022.106055>

Zahlan, H., Groeneveld, D., Tavoularis, S., 2015, "Fluid-to-fluid scaling for convective heat transfer in tubes at supercritical and high subcritical pressures", *Int. J. Heat Mass Transfer*, 73, 274–283.  
<https://doi.org/10.1016/j.ijheatmasstransfer.2014.02.018>

Zahlan, H., Tavoularis, S., Groeneveld, D., 2015a. "A look-up table for trans-critical heat transfer in water-cooled tubes" , *Nucl. Eng. Des.* 285, 109–125.

<https://doi.org/10.1016/j.nucengdes.2014.12.027>

Zahlan, H., Groeneveld, D., Tavoularis, S., 2015b. "Measurements of convective heat transfer to vertical upward flows of CO<sub>2</sub> in circular tubes at near-critical and supercritical pressures", *Nucl. Eng. Des.* 289, 92–107.  
<https://doi.org/10.1016/j.nucengdes.2015.04.013>